Article

Simple Multifunctional PTX@Ce6 Nanomedicine for Eradicating Tumor in the Combination of Photodynamic Therapy and Metronomic Chemotherapy

Mengxuan Li,[†] Ge Cheng,[†] Rui Zhang,* and Juan Li*

Read Online

ACCESS | Metrics & More | Article Recommendations

ABSTRACT: Photodynamic therapy (PDT) is an effective treatment modality for various cancer types. However, tumor recurrence and metastasis stemming from residual cancer cells after PDT pose serious problems. In this study, a simple multifunctional PTX@Ce6 nanomedicine is prepared using a two-step reprecipitation method. In this core−shell nanostructure, the toxic paclitaxel (PTX) core is embedded into a nontoxic Ce6 shell. An ultralow dose of PTX (1 mg/kg) stimulates the differentiation of marrow-derived suppressor cells (MDSCs) into mature dendritic cells (DCs), resulting in the restoration of functions of tumor-specific CD8$^+$ T cells and promotion of antitumor immune responses in vivo. Hence, the tumors in mice are eradicated with 100% tumor inhibition rate via combination therapy. Tumor recurrence and metastasis are also effectively inhibited. In addition, the combination therapy with PDT and metronomic chemotherapy based on core−shell PTX@Ce6 nanostructures shows high biosafety in treated mice. This study can aid in developing new cancer treatment modalities for eradicating tumors, preventing tumor recurrence and metastasis, and reducing the systemic side effects of therapy.
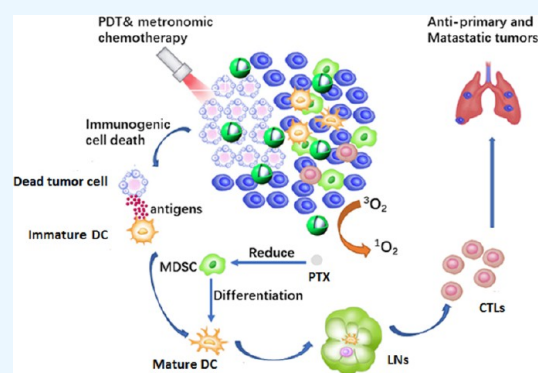
1. INTRODUCTION

Multifunctional nanomedicines are considered crucial for cancer therapy owing to their outstanding performance, such as high drug loading capacity,[1] effective targeting of tumor sites,[2,3] smart release of therapeutics,[4−6] and reduced side effects.[7] Due to their superiority to individual functional nanomedicines, multifunctional nanomedicines have gained attention in tumor treatment.[8] However, there are some challenges in the effective design of multifunctional nanomedicines.[9] One major challenge is the complexity of multifunctional nanomedicines that leads to high cost of production, low repeatability in preparation, and difficulty in achieving clinical translation.[10−12] Moreover, excipients are generally used for preparing multifunctional nanomedicines, resulting in unsatisfactory drug loading ratios.[13,14] Recently, excipient-free nanomedicines have attracted wide attention for tumor treatment.[15−17] There is a strong demand for the development of multifunctional nanomedicines with simple compositions without any excipients via simple methods.

In photodynamic therapy (PDT), photosensitizers (PSs) are irradiated by visible or near infrared light to generate toxic reactive oxygen species (ROS), specifically singlet oxygen ($^1O_2$), at tumor sites.[18,19] PDT is an effective treatment modality for various cancers.[20−24] The antitumor mechanism of PDT involves the generation of $^1O_2$, which is a toxic species

that can kill tumor cells via cellular apoptosis and/or necrosis path, at tumor sites. However, tumor recurrence caused by residual cancer cells after PDT poses a serious problem.[25] To eradicate tumors and prevent metastasis of residual cancer cells, combining PDT with other therapies, such as chemotherapy and immune therapy, is considered an ideal treatment modality.

Paclitaxel (PTX) is one of the most important chemotherapeutic anticancer medicines that is used for the first-line treatment of various cancers, such as breast, non-small cell lung, and ovarian cancers.[26−28] PTX suppresses tumor growth by stabilizing the microtubule and inhibiting the mitosis of tumor cells. However, dose-dependent side effects caused by the systemic administration of PTX still pose a serious problem for patients with cancer. Usually, chemotherapy for cancers with PTX is based on the maximum-tolerated dose (10 mg/kg/week), resulting in severe toxicity, drug resistance, and strong immunosuppression. Metronomic chemotherapy can

reduce the systemic side effects of PTX.[29] Metronomic chemotherapy is defined as the frequent administration of chemotherapeutic agents at nontoxic doses. Michels et al. proved that PTX delayed the growth of melanoma in mice using an ultra-low-dose in vivo, as indicated by the decrease in the number of infiltrated marrow-derived suppressor cells (MDSCs) in tumors.[30] Condamine and Gabrilovich revealed that MDSCs can inhibit the proliferation and activation of T cells by secreting interleukin IL-10 and downregulating the maturation and function of murine and human dendritic cells (DCs).[31]

Based on the abovementioned results, we propose a new cancer treatment strategy that combines PDT and metronomic chemotherapy. This combined treatment modality may not only generate $^1O_2$ to kill most tumor cells but also initiate the antitumor immune response of the host to kill the residual tumor cells, eradicate tumors, prevent tumor recurrence and metastasis, and reduce the systemic side effects.

In this study, we prepared a simple multifunctional core–shell PTX@Ce6 nanomedicine with 100% drug loading rate using a simple two-step reprecipitation method. The PTX core endows the functions of chemotherapeutics and immunomodulators for 4T1 tumors, while the Ce6 shell as a PS implements PDT of tumors and tumor vaccine-like function under 660 nm laser irradiation. Combination therapy using PTX@Ce6 led to tumor eradication and prevention of tumor recurrence and metastasis in 4T1 tumor-bearing mice. Moreover, systemic side effects induced by traditional cancer chemotherapy were greatly reduced. Our findings can be used to develop new cancer treatment modalities for the eradication of tumors and prevention of tumor recurrence and metastasis in affected patients. The preparation method of PTX@Ce6 nanoparticles (NPs) and the mechanism of the combined treatment of tumors are illustrated in Scheme 1.

2. EXPERIMENTAL SECTION

2.1. Preparation and Characterization of PTX@Ce6 NPs. To prepare PTX@Ce6 NPs, a two-step reprecipitation method was used. Specifically, 400 μL of PTX solution in tetrahydrofuran (THF; 0.2 mg/mL^{-1}) was added to 5 mL of deionized water under vigorous stirring at 25 °C for 10 min. Then, 800 μL of Ce6 solution in acetone (0.2 mg/mL^{-1}) was added to the dispersion containing PTX cores for 20 min to form core–shell PTX@Ce6 NPs. After further stirring for another 2 h, THF and acetone in the mixture were allowed to evaporate via nitrogen blubbing. PTX and Ce6 NPs were prepared using the reprecipitation method. The morphologies and sizes of the three NPs were determined via TEM (FEI TecnaiG2 S-Twin). The hydrodynamic sizes and zeta potentials of the three NPs were detected in aqueous dispersions via dynamic light scattering (DLS).

2.2. Release of PTX from PTX@Ce6 NPs at Different pH. Cumulative release of PTX from PTX@Ce6 NPs was carried out via dialysis plus high-performance liquid chromatography (HPLC). A dialysis membrane with 3.5 kDa MW cutoff containing the PTX@Ce6 NP dispersion was put into 40 mL of phosphate-buffered saline (PBS) solution (0.05% Tween 20) and dialysis was performed at pH 6.0, 7.0, and 7.4. Then, 1 mL of the dialysate was removed and measured using HPLC. Finally, 1 mL of the dialysate was returned to PBS solution to maintain the original volume.

2.3. Evaluation of the $^1O_2$ Generation Ability of Ce6 and PTX@Ce6 NPs. $^1O_2$ generation by Ce6 and PTX@Ce6

Scheme 1. Schematic of the Synthesis of Core–Shell PTX@Ce6 Nanomedicine and Their Antitumor Mechanism in Combination Treatment[a]
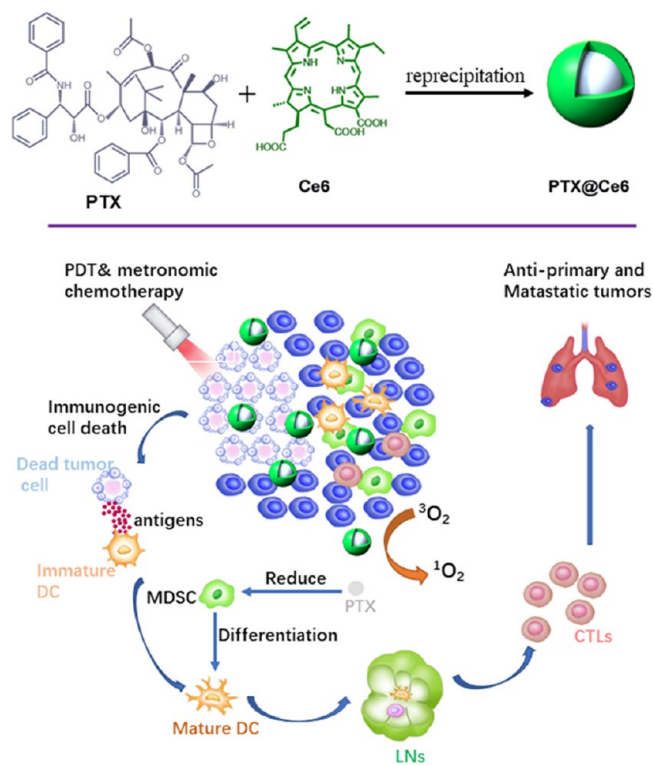
[a]PDT and metronomic chemotherapy induce the apoptosis and necrosis of tumor cells, followed by the release of tumor-associated antigens (TAAs). Immature dendritic cells (DCs) become mature via the processing and presentation of TAAs. Then, mature DCs migrate to the lymph node and promote the transformation of naïve T cells to effector T cells. Then, effector T cells migrate and infiltrate into the tumor microenvironment (TME). Ce6 can generate singlet oxygen ($^1O_2$) under irradiation and PTX can differentiate MDSCs to mature DCs.

NPs was investigated using singlet oxygen sensor green (SOSG) as an indicator with a 660 nm laser. First, 3 mL of Ce6 or PTX@Ce6 NP aqueous dispersion (containing 0.02 mg/mL of Ce6) was mixed via adding 60 μL of SOSG aqueous solution with a concentration of 1 mg/mL. The liquid mixtures were illuminated using a 660 nm laser (0.5 W cm^{-2}) for various periods up to 45 min. The generation of singlet oxygen in the illuminated samples was then determined according to the change of fluorescence intensity of oxidized SOSG.

2.4. Generation of Intracellular ROS. First, 4T1 cells were seeded into a 96-well plate at a density of 5×10^3 cells/well and the plate was incubated for 12 h. Then, the culture medium in each well was removed and then replaced with 100 μL of Ce6 or PTX@Ce6 NP dispersion diluted with the culture medium. After incubation for 4 h, 20 μL of DCFH-DA (0.03 mg/mL) was added to the medium and cultured for another 30 min, followed by illumination with a 660 nm laser (0.5 W cm^{-2}) for 10 min. Finally, the cells were washed with PBS and imaged using an inverted fluorescence microscope (Olympus).

2.5. In Vitro Cell Imaging of PTX@Ce6 NPs. To observe the internalization and distribution of PTX@Ce6 NPs in 4T1 tumor cells, in vitro cell images of PTX@Ce6 NPs were collected using Ce6 NPs as controls. Briefly, 4T1 cells were
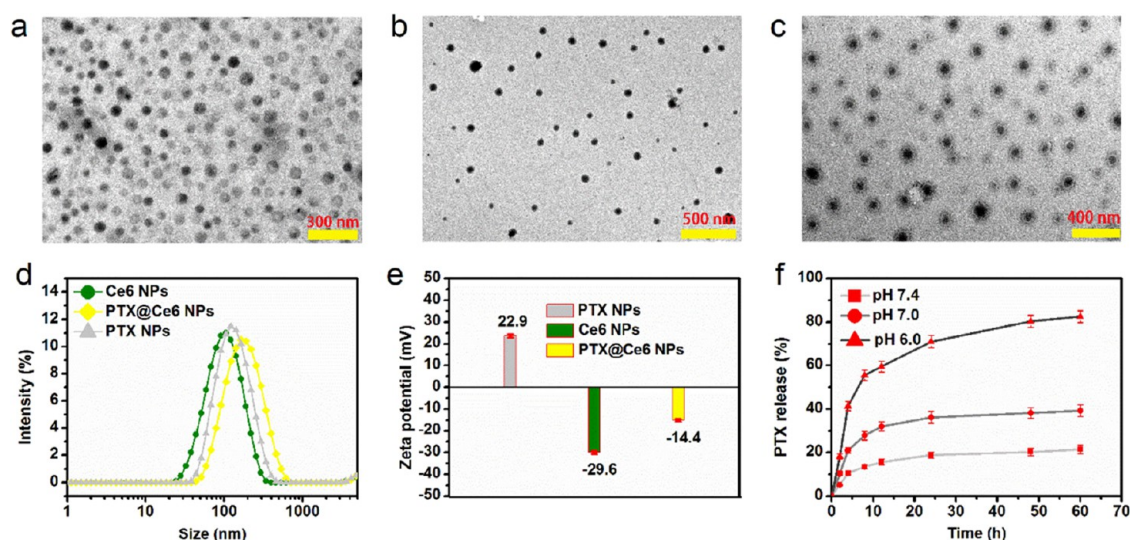
Figure 1. Characterization of three nanoparticles (NPs). (a–c) TEM images of chlorin e6 (Ce6), paclitaxel (PTX), and PTX@Ce6 NPs. (d) Hydrodynamic diameter distribution of Ce6, PTX, and PTX@Ce6 NPs. (e) Zeta potentials of PTX, Ce6, and PTX@Ce6 NPs measured by DLS. (f) Cumulative release of PTX from PTX@Ce6 NPs at pH 6.0, 7.0, and 7.4.

cultured under standard conditions in a humidified incubator. Trypsinized 4T1 cells were resuspended and seeded into a 24-well plate, followed by incubation for 24 h. Ce6 or PTX@Ce6 NP dispersion was added to each plate. Treated 4T1 cells in the two samples were incubated for 4 h under the same treatment conditions. After thoroughly washing with PBS, the 4T1 cells were imaged using an Olympus inverted fluorescent microscope.

2.6. In Vitro Cytotoxicity. Briefly, 4T1 cells were seeded into a 96-well plate at a density of 2×10^3 cells/well and Ce6 or PTX@Ce6 NP dispersion was added into wells with a setting concentration. The 96-well plate was incubated for 10 h. Then, 4T1 cells were illuminated using a 660 nm laser for 8 min under 0.5 W cm^{-2}. After illumination, the cells were incubated for another 14 h. For PTX NPs, 4T1 cells were not illuminated and continuously incubated for 24 h. In vitro cytotoxicity was detected using standard MTT assay.

2.7. Antitumor Activity in the 4T1 Model. Female BALB/c mice (6-week-old) were used as test animals. First, 5 × 10^5 4T1 cells were subcutaneously injected into the right flank of each of mice. When the average tumor volumes reached ~60 mm^3, the 4T1 tumor-bearing mice were randomly divided into four groups (five mice per group): (1) PBS, (2) PTX NPs, (3) Ce6 NPs with irradiation, and (4) PTX@Ce6 NPs with irradiation groups. PTX, Ce6, and PTX@Ce6 NPs were injected via the tail vein into mice at a Ce6 dose of 2 mg kg^{-1} and/or at a PTX dose of 1 mg kg^{-1} every two days for a total of seven injections. Eight hours after each injection, the mice in (3) and (4) groups were anesthetized with 2% (v/v) isoflurane and tumors were illuminated using a 660 nm laser (0.5 W cm^{-2}) for 8 min. To avoid any lesions of the outer skin of mice, the irradiation distance from the tumor of mice to laser exit was set to be 30 cm. At this distance, outer skin of mice did not have lesions under the irradiation of 660 nm laser (0.5 Wcm^{-2}). Then, 4T1 tumor volumes and body weights of mice were monitored every two days for a total of 14 days. The tumor volumes were calculated as follows: (width^2 × length)/2. At the end of the experiment, the mice were euthanized, and the tumors were excised, weighed, and photographed.

2.8. Evaluation of Tumor Lung Metastases. In another 20 female BALB/c mice (6-weeks-old), antitumor experiments were performed according to the experimental steps mentioned above (Section 2.7). At the end of the experiment on day 24 after initial treatments, the mice from four groups were euthanized and lungs were excised, and tumor nodules on the subsurface of the lungs were counted. The lungs were sectioned and subjected to hematoxylin and eosin (H&E) staining.

2.9. Evaluation of Tumor Apoptosis and ICD In Vivo. To evaluate the apoptosis and immunogenic cell death (ICD) of 4T1 tumor cells, on day 10 after the initial treatment, the mice were sacrificed, and tumors were removed, sectioned, and stained with Alexa Fluor 488-conjugated anti-calreticulin (CRT) antibody and TUNEL assay. Finally, ICD and apoptosis of 4T1 tumor cells in vivo were detected by fluorescence microscopy analysis.

2.10. Tumor Rechallenge Study. Effects of PTX@Ce6 NPs on immune memory were evaluated using a tumor rechallenge study. The mice were divided into two groups (n = 5): (1) the PTX@Ce6 NPs (+) group, in which the initial tumors were eliminated via combination therapy using PTX@Ce6 NPs plus 660 nm laser irradiation on day 14 and (2) the PBS group, in which the initial tumors were removed via surgery on day 14. On day 21, 5 × 10^5 4T1 cells were subcutaneously injected into the right flank of female BALB/c mice in the two groups. After the cells were inoculated for seven days, approximately 60 mm^3 size tumors were formed in the mice. Additional intravenous injections of PTX@Ce6 NPs were given at a dose of 1 mg/kg for PTX and 2 mg/kg for Ce6 plus irradiation five times from 28 to 36 d for (1) group every other day. In (2) group, the mice did not receive any treatment. On day 48, mice from both groups were euthanized, and the tumors were excised and weighed.

2.11. Biosafety of Combination Therapy Based on PTX@Ce6 NPs. At the end of the in vivo anti-tumor experiment, the treated mice were sacrificed, the blood samples were collected, and the heart, lungs, liver, spleen, and kidneys were removed. Blood analysis and H&E images of
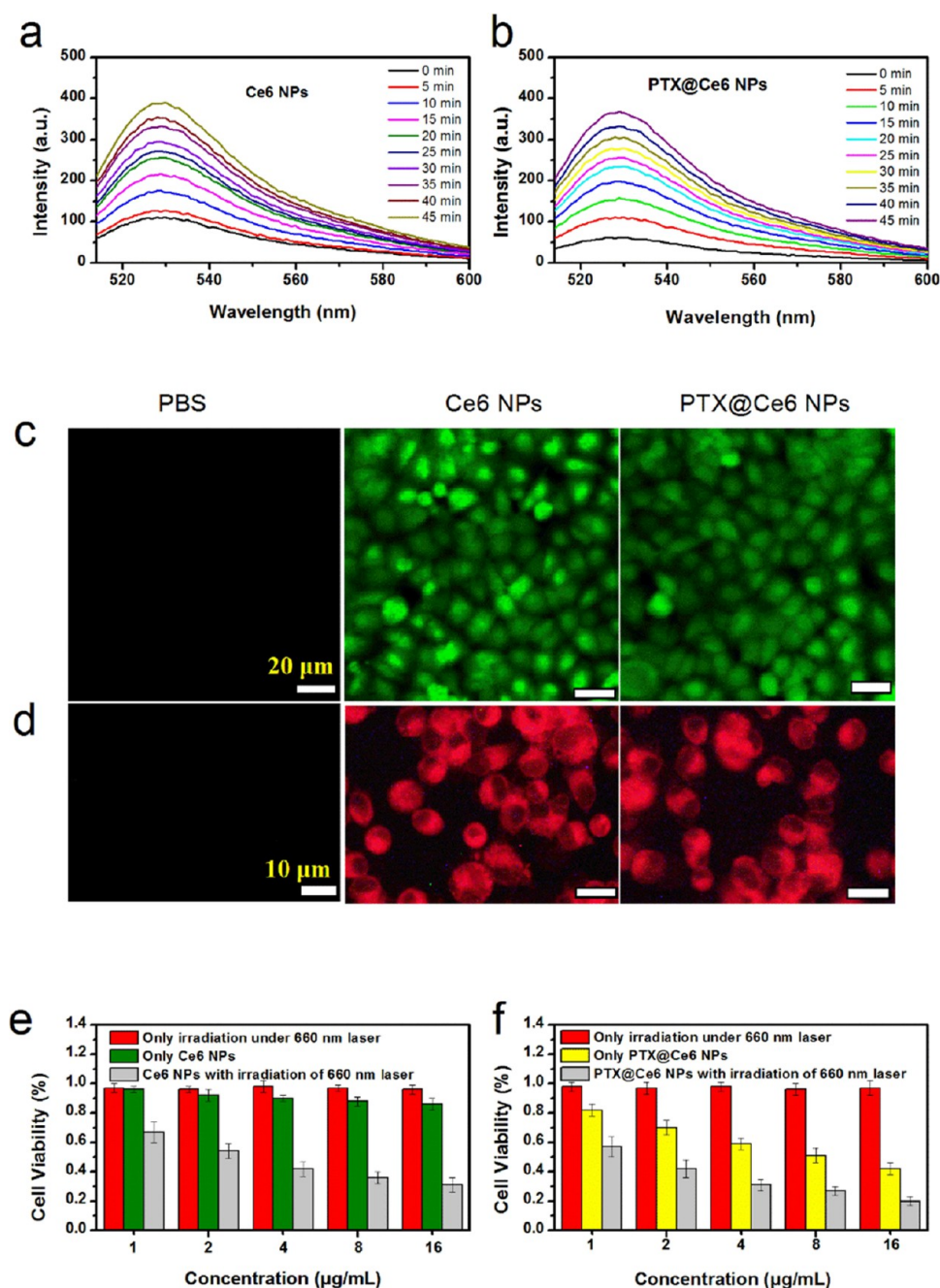
Figure 2. (a,b) Fluorescence spectra of SOSG solution incubated with Ce6 NPs and PTX@Ce6 NPs with the same concentration of Ce6 (2 μg/mL) after irradiation with a 660 nm laser. (b) Fluorescence images of intracellular ROS detected using the DCFH-DA probe. (d) Fluorescence images of 4T1 cells showing the released Ce6 molecules from Ce6 or PTX@Ce6 NPs into the cytoplasm. (e) 4T1 cell viabilities at different conditions: only irradiation, only Ce6 NPs, and Ce6 NPs plus irradiation. (f) 4T1 cell viabilities at different conditions: only irradiation, only PTX@Ce6 NPs, and PTX@Ce6 NPs plus irradiation.

major organs were completed according to conventional methods.

2.12. Study Approval. All animal experiments were performed and approved at the Institute of Radiation Medicine (Tianjin, China) and adhered to the guidelines of the Committee for Research and Animal Ethics.

2.13. Statistical Analysis. All results were presented as means ± SD. Differences between groups were analyzed by the two-tailed Student's *t*-test using GraphPad Prism software. The differences with $*p < 0.05$, $**p < 0.01$, and $***p < 0.001$ were considered statistically significant.

3. RESULTS AND DISCUSSION

3.1. Preparation and Characterization of Three NPs. In this study, we aimed to prepare a potent multifunctional PTX@Ce6 nanomedicine that can be employed in combination with PDT and metronomic chemotherapy for 4T1 tumors. Due to the high hydrophobicity and poor water solubility of PTX and Ce6, core−shell PTX@Ce6 NPs were prepared using a two-step reprecipitation method. First, the PTX core was formed by rapidly dropping a THF solution containing PTX into water with rapid stirring. Then, an acetone solution of Ce6 was dropped into an aqueous
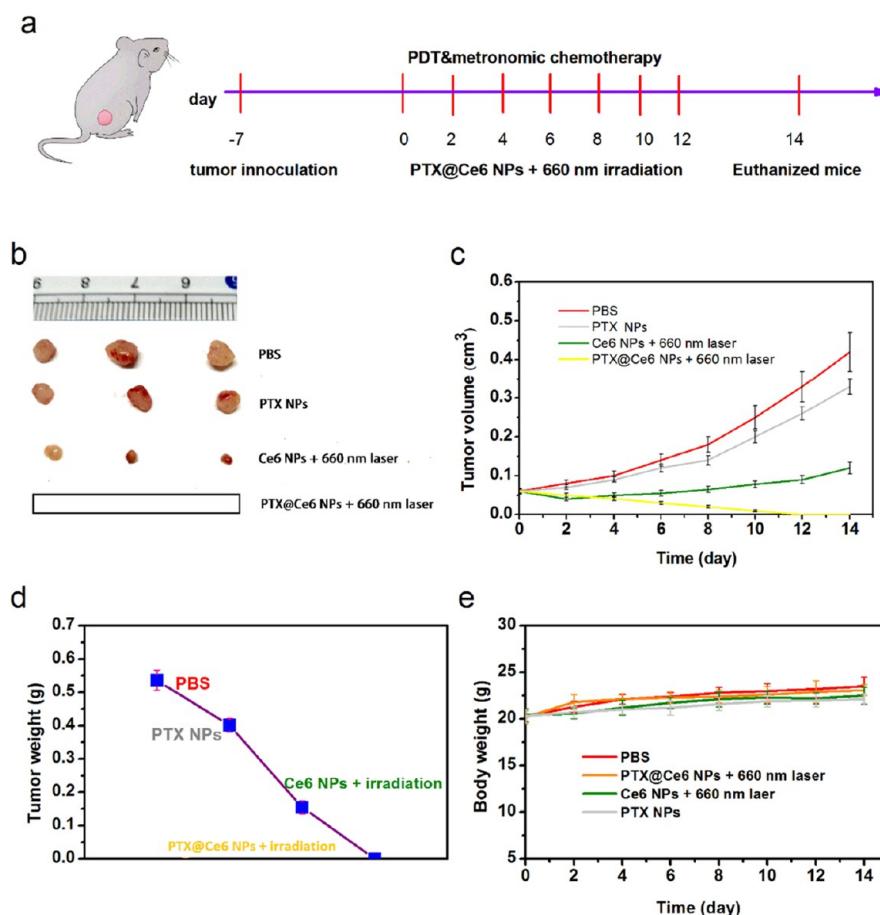
Figure 3. (a) Schedule for PTX@Ce6 NP-mediated combination therapy with PDT and metronomic chemotherapy. (b) Photographs of removed tumors at the end of the experiment. (c) Tumor volumes of tumor-bearing mice after various treatments for 14 days. (d) Changes in tumor weights after various treatments. (e) Body weight of tumor-bearing mice during 14 days of various treatments.

dispersion of PTX cores to form core−shell PTX@Ce6 NPs. In this core−shell nanostructure, the toxic PTX core is embedded into a nontoxic Ce6 shell, which is conducive to reducing the side effects of PTX in PTX@Ce6 NPs during blood circulation. PTX and Ce6 NPs were also prepared by the reprecipitation method and used as controls.

TEM images of Ce6 NPs, PTX NPs, and PTX@Ce6 Ps are shown in Figure 1a−c. The spherical nanoparticles with average sizes of 86 ± 9 nm for Ce6 NPs and 143 ± 11 nm for PTX NPs were observed. The core−shell PTX@Ce6 NPs were 195 ± 16 nm in size, as shown in the TEM image. The image also shows PTX cores with diameters of ∼135 ± 8 nm and Ce6 shells with thicknesses of ∼30 ± 5 nm. DLS measurements (Figure 1d) showed hydrodynamic diameters of 91 ± 10 nm for Ce6 NPs, 148 ± 10 nm for PTX NPs, and 201 ± 18 nm for PTX@Ce6 NPs, which are similar to the results of Transmission electron microscopy (TEM). PTX NPs had positive zeta potentials (22.9 mV) and Ce6 NPs had negative zeta potentials of −29.6 mV (Figure 1e). Therefore, PTX@Ce6 NPs were easily formed through electrostatic attraction in the two-step reprecipitation method.

PTX release from PTX@Ce6 NPs was monitored by HPLC at pH 6.0, 7.0, and 7.4, respectively. At pH 6.0, corresponding to the tumor microenvironment, the release rate of PTX reached over 80% after 60 h (Figure 1f). At physiological pH 7.4, PTX@Ce6 NPs were stable and generated a slight release.

3.2. Generation of ROS, Cellular Localization, and Cytotoxicity.
PS can generate cytotoxic $^1O_2$ through a type II reaction, in which the excited triplet state of PS can transfer energy directly to $^3O_2$ to generate $^1O_2$. It is well known that Ce6 is an excellent PS when irradiated with red light. $^1O_2$ generation from Ce6 NPs and PTX@Ce6 NPs under 660 nm laser irradiation was measured using SOSG as the detection probe.[32] Mixtures of SOSG and Ce6 NP dispersion or PTX@Ce6 NP dispersion were respectively irradiated with 660 nm laser at 0.5 W cm^{-2}. When Ce6 NP dispersion and PTX@Ce6 NP dispersion contained the same concentration of Ce6 (0.05 mg/mL), the fluorescence intensities of the oxidized SOSG peaked at 525 nm increased with irradiation time with similar trends for the two NPs, indicating that PTX in PTX@Ce6 has no negative influence on the $^1O_2$ generation capacity of Ce6 (Figure 2a,b).

Considering the $^1O_2$ generation capacities of Ce6 NPs and PTX@Ce6 NPs, the intracellular photodynamic activity of Ce6 NPs and PTX@Ce6 NPs was then investigated using DCFH-DA as the ROS probe. The results indicate that the 4T1 cells emitted intracellular green fluorescence of DCFH-DA due to the generation of ROS.[33] In contrast, when the 4T1 cells were incubated with PBS plus 660 nm laser irradiation, almost no green fluorescence was observed (Figure 2c). To investigate cell endocytosis of Ce6 NPs and PTX@Ce6 NPs, 4T1 cells were incubated with Ce6 NPs or PTX@Ce6 NPs at the same concentration of Ce6 (2 μg/mL). Obviously, subcellular red
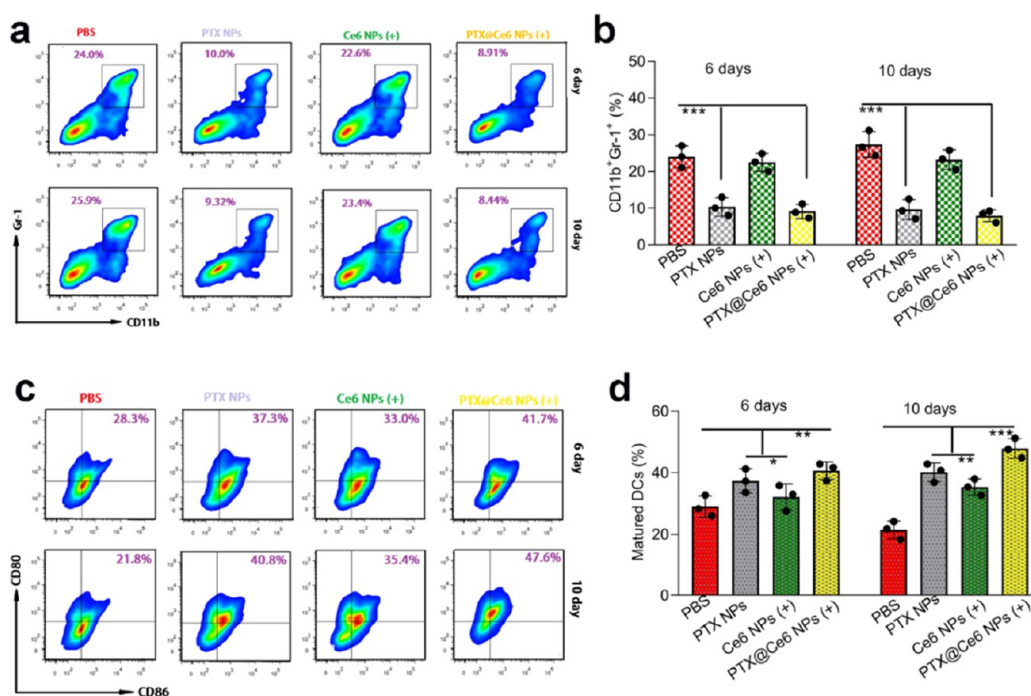
Figure 4. Flow cytometry analysis of MDSCs and DCs on days 6 and 10 after initial treatment. (a) Representative frequency of MDSCs (CD11b$^+$Gr-1$^+$). (b) Quantitative frequency of MDSCs. (c) Representative frequency of mature DCs (CD80$^+$CD86$^+$). (d) Quantitative frequency of mature DCs.

fluorescence confirmed endocytosis of the Ce6 NPs or PTX@Ce6 NPs into the cytoplasm (Figure 2d).

Photocytotoxicity of as-prepared PTX@Ce6 NPs was determined by comparing the viability of 4T1 cells in three cohorts: (1) irradiated with 660 nm laser only (red bars), (2) incubated with PTX@Ce6 NPs only (yellow bars), and (3) irradiation + PTX@Ce6 NPs (gray bars). Apparently, the irradiation alone does not have any cytotoxicity and the cell viability of PTX@Ce6 NPs was 42% due to the fact that PTX has cytotoxicity and Ce6 has less cytotoxicity when the concentration of PTX@Ce6 NPs was 16 μg/mL. Moreover, with 660 nm laser irradiation, the cell viability of PTX@Ce6 NPs further reduced to 21% (Figure 2e). In contrast, the cell viability of Ce6 NPs at a concentration of 16 μg/mL under 660 nm laser irradiation was 32% (Figure 2f).

3.3. Antitumor Activity of Combination Therapy. Based on the $^1O_2$ generation capacity and photocytotoxicity of PTX@Ce6 NPs, the antitumor effect of PDT combined with metronomic chemotherapy based on PTX@Ce6 NPs for 4T1 tumor was investigated. The right flanks of female BALB/c mice were subcutaneously injected with 5×10^5 4T1 cells. After the cells were inoculated for seven days, the tumor volumes reached approximately 60 mm^3. The tumor-bearing mice were randomly divided into four groups (five mice per group n): (1) PBS, (2) PTX NPs only, (3) Ce6 NPs plus 660 nm laser irradiation, and (4) PTX@Ce6 NPs plus 660 nm laser irradiation. PTX NPs (200 μL), Ce6 NPs, or PTX@Ce6 NPs at a dose of 1 mg kg^{-1} for PTX and 2 mg kg^{-1} for Ce6 were intravenously injected into corresponding mice, every other day seven times. The therapeutic schedule is illustrated in Figure 3a. On day 14, all test mice were sacrificed, and the corresponding tumors were removed. Figure 3b shows the photographs of the excised tumors from euthanized mice. The tumor volumes in mice treated by PDT with Ce6 NPs are smaller than those treated by metronomic chemotherapy with

PTX NPs. In particular, the tumors in the mice treated with combination therapy based on PTX@Ce6 NPs were eradicated with 100% tumor inhibition rate (Figure 3b−d). Several previous studies have reported combination therapies based on Ce6 and chemotherapeutic medicines against cancer cells and tumors.[34−37] However, treated tumors were not completely eliminated. In addition, body weights were stable in the test mice treated with different treatment modes, indicating negligible side effects of PTX NPs, Ce6 NPs (+), and PTX@Ce6 NPs (+) for tumor therapy at the employed dose (Figure 3e). (+) refers to 660 nm laser irradiation (0.5 W/cm^2).

PDT of tumors represents a promising solution for treating solid tumors. However, it usually suffers from incomplete tumor killing owing to residual tumor cells, which ultimately leads to tumor recurrence and metastasis. In this study, we combined metronomic chemotherapy with PDT, and 4T1 tumors were completely eliminated by PTX@Ce6 NPs under 660 laser illumination. Many previous studies have indicated that PDT could only inhibit tumor growth but not completely eliminate tumors.[38−41] The main low-dose PTX (1 mg kg^{-1}) differentiated MDSCs to mature DCs that activated effector T cells that infiltrated the tumor microenvironment and killed residual tumor cells. The following experimental results prove our conclusions.

3.4. Antitumor Mechanism of Combination Therapy. PTX is an effective chemical anticancer medicine when used at the maximum-tolerated dose (MTD, 10 mg kg^{-1} week^{-1}) in conventional chemotherapy for breast cancer. However, MTD not only causes toxic side effects in normal organs but also inhibits host immunity. Interestingly, in this study, we used metronomic chemotherapy to replace MTD chemotherapy with PTX NPs or PTX@Ce6 NPs *in* the 4T1 tumor model. PTX NPs (200 μL), Ce6 NPs, or PTX@Ce6 NPs (1 mg kg^{-1} for PTX and 2 mg kg^{-1} for Ce6) were intravenously injected
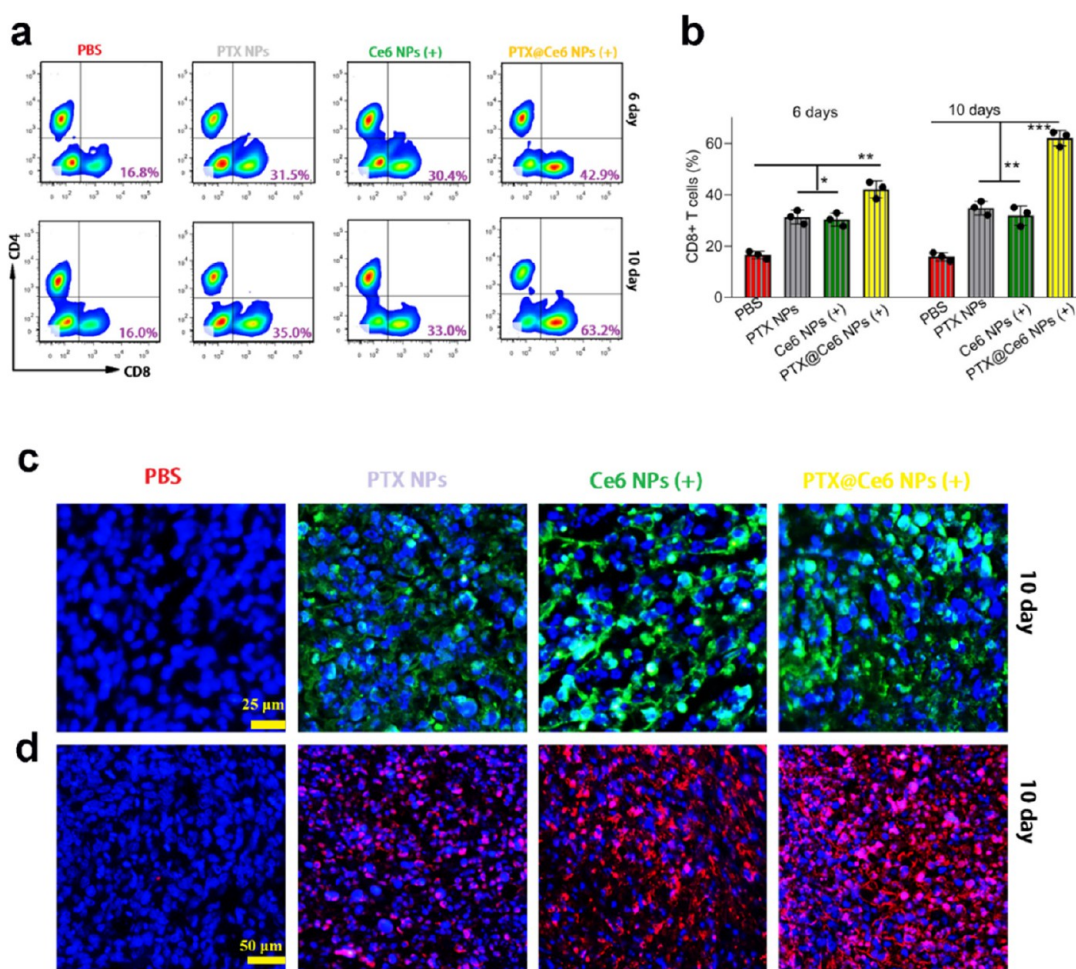
Figure 5. (a) Representative frequency of CD8$^+$ T cells (CD3$^+$CD8$^+$CD4$^-$). (b) Quantitative frequency of CD8$^+$ T cells. (c) Immunofluorescence images of CRT in vivo. (d) TUNEL images of tumor cell apoptosis in different groups in vivo.

into corresponding tumor-bearing mice, respectively, every other day seven times. Then, the mice in (3) and (4) groups were irradiated with 660 nm laser. During the treatment of 4T1 tumors, the frequencies of MDSCs and DCs in the TME at 6 and 10 d after initial treatments were measured by flow cytometry. The results showed that the percentage of MDSCs (CD11b$^+$Gr-1$^+$ cells) in tumors deceased in all three treatment groups. Especially, in the PTX@Ce6 NP plus irradiation group, the frequency of MDSCs was more obviously downregulated, and the percentage of MDSCs was significantly reduced to 8.91% compared with 24.0% in the PBS group on day 6 (Figure 4a,b). Notably, the percentage of MDSCs in the PTX NP group was lower than that in the Ce6 NP plus irradiation group, indicating that low-dose PTX plays a pivotal role in MDSC depletion. A similar trend in the depletion of MDSCs in the tumor microenvironment (TME) also was observed on the 10th day after various treatments. Compared with 6th day, the depletion of MDSCs became more obvious in the corresponding treatment groups, except in the PBS group.

To assess DC maturation, the cells in the draining lymph nodes were collected from 4T1 tumor-bearing mice after various treatments. Compared to the PBS group, the other three groups displayed an obvious increase in mature DCs. Especially, for the PTX@Ce6 plus irradiation group, the percentage of mature DCs (CD11c$^+$CD80$^+$CD86$^+$) was significantly improved up to 41.7% and 47.6% from 28.3%

and 21.8% of the PBS group on days 6 and 10, respectively (Figure 4c,d). Thus, we can conclude that PTX at an ultra-low-dose (1 mg/kg) stimulated MDSC differentiation toward DC, and PDT can synergistically improve the stimulatory effect. MDSC can suppress tumor immunity via a variety of mechanisms, including perturbing T-cell activation and blocking the proliferation of T cells.[42] Therefore, a decrease in MDSC obviously improves antitumor immune responses in hosts, resulting in a direct antitumor effect.

The decrease in MDSC numbers restored the functions of tumor-specific CD8$^+$ T cells and promoted CD8$^+$ T-cell-dependent antitumor immunity responses in vivo.[43] In this work, the reduction in MDSC was accompanied by the maturation of the DCs and recognition of tumor cells by the tumor-specific antigen. Thus, the antitumor effect of PTX is associated with the restoration of CD8 T$^+$ cell activity. We next measured the frequency of CD8$^+$ T cells in 4T1 tumors on days 6 and 10 after various treatments using flow cytometry. The results indicated that the frequency of CD8$^+$ T cells (CD3$^+$CD8$^+$CD4$^-$) in tumors was upregulated in all three treatment groups. The PTX@Ce6 NP plus irradiation group displayed the most obvious increase (Figure 5a,b). The percentage of CD8$^+$ cells in tumors was significantly enhanced to 42.9% from 16.8% of the PBS group on day 6. On day 10, corresponding values are from 16.0 to 63.2%. Notably, in the PTX NP group and the PDT group with Ce6 NPs, similar
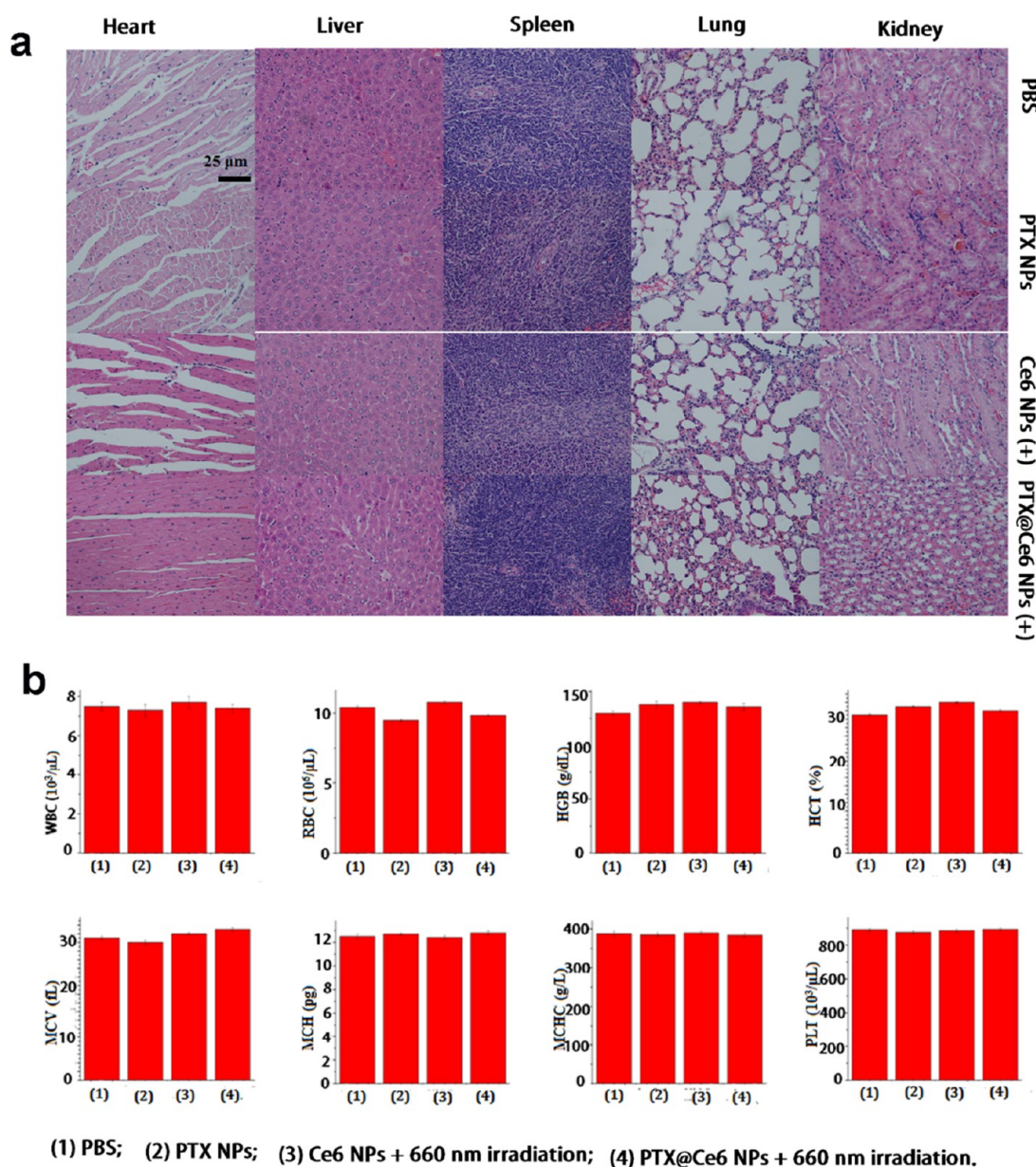
Figure 6. (a) Images of the heart, liver, spleen, lung and kidney histological sections from various treatment groups. (b) Complete blood panel data from the groups of control and treatment.

increases in CD8$^+$ T cells were observed on days 6 and 10 post-treatment, respectively. These results showed that PDT with Ce6 and metronomic low-dose chemotherapy with PTX for 4T1 tumors induced the proliferation of CD8$^+$ cells. The former acts primarily via the induction of ICD by PDT, whereas the latter acts mainly by depleting MDSCs.

The antitumor mechanism of PTX involves a cell apoptotic pathway at low doses. Thus, it is expected that PTX NPs at low doses will likely induce ICD. The secretion of CRT on the surface of apoptotic tumor cells is regarded as a feature of ICD. Therefore, CRT expression around 4T1 tumor cells was measured on day 10 post-treatment. The secretion of CRT on the surfaces of 4T1 cells was observed in three groups, including PTX NPs, Ce6 NPs (+), and PTX@Ce6 NPs (+), due to CRT emitting green fluorescence. Bright green was found in the PDT group based on PTX@Ce6 NPs (+) (Figure 5c).

On the other hand, 4T1 tumor sections were stained via TUNEL assay to confirm the death of 4T1 cells. The tumor treated with PTX NPs shows clear cell apoptosis because of the red fluorescence around the blue nucleus, and the most severe cell apoptosis was found in the combination treatment group based on PTX@Ce6 NPs (+) owing to the large number of red fluorescence dots in the TUNEL image (Figure 5d). These results indicate that metronomic chemotherapy with ultralow noncytotoxic doses of PTX can be combined with PDT to reverse immunosuppression in the tumor microenvironment, thereby increasing the antitumor efficiency.

3.5. Biosafety of Combination Therapy. The dose-dependent systemic side effects of PTX pose a challenge in treatment. We designed a novel combination therapy with PDT and metronomic chemotherapy using a core−shell PTX@Ce6 nanostructure to ablate 4T1 tumors without any systemic side effects. To evaluate the in vivo biosafety of the combined treatment, after 14 d of various treatments, healthy

organs, including the heart, liver, spleen, lungs, and kidneys, were excised from 4T1 tumor-bearing mice in PBS, PTX NPs, Ce6 NPs (+), and PTX@Ce6 NPs (+) groups. We then collected H&E-stained images of these organs (Figure 6a). In all groups, no noticeable organ damage or inflammatory lesions were found, suggesting no observable liver, lungs, spleen, heart, or kidney dysfunction in mice.

Blood analysis data of tumor-bearing mice from the treatment and control groups were obtained. No observable toxicity was observed in the blood (Figure 6b). These results demonstrated that the combination therapy with PDT and metronomic chemotherapy using a sample core−shell PTX@Ce6 nanostructure had high biosafety in the treated mice.

3.6. Prevention of Tumor Recurrence and Metastasis by Combination Therapy. PDT can effectively inhibit tumor growth but cannot completely eliminate the tumors. Residual cancer cells after PDT can result in tumor recurrence and metastasis. In this study, 4T1 tumors were completely eliminated by combining PDT with metronomic chemotherapy using PTX@Ce6 NPs. We investigated tumor recurrence after the elimination of the initial tumors using the tumor rechallenge test (Figure 7a).

The mice were divided into two groups ($n = 5$): (1) the PTX@Ce6 NPs (+) group, in which the initial tumors were eliminated via combination therapy using PTX@Ce6 NPs plus 660 nm laser irradiation on day 14 and the (2) PBS group, in which the initial tumors were removed via surgery on day 14. On day 21, 5×10^5 4T1 cells were subcutaneously injected

into the right flank of female BALB/c mice in the two groups. After 4T1 cells were inoculated for seven days, approximately 60 mm^3 size tumors were formed in the mice. Additional intravenous injections of PTX@Ce6 NPs were given at a dose of 1 mg/kg for PTX and 2 mg/kg for Ce6 plus irradiation five times from 28 to 36 d for (1) group. In (2) group, the mice did not receive any therapy. The growth of the rechallenged tumors was evaluated from 28 to 48 d. Compared with tumors in the untreated group, the growth of rechallenged tumors in the PTX@Ce6 NPs (+) group was significantly inhibited, only one of five mice had a rechallenged tumor of 15 mm^3 and the inhibition rate of the rechallenged tumors was 99.7% (Figure 7b,h). These results demonstrated that a long-term protective immune memory response was induced by the combination therapy with PDT and metronomic chemotherapy using PTX@Ce6 NPs. The survival rates of mice were monitored after the rechallenge tumors were therapied, and 80% of the mice survived over 70 d in PTX@Ce6 NPs plus irradiation group (Figure 7c).

The increase of memory T cells (T_{EM} cells) are very important to preventing tumor recurrence. T_{EM} images of cells in the spleens of the untreated and PTX@Ce6 NPs (+) groups were analyzed via flow cytometry on day 30. Compared to 19.2% T_{EM} cells in the untreated group, the percentage of T_{EM} cells in the PTX@Ce6 NPs (+) group reached 49.4% (Figure 7d,e). Therefore, the combination of PDT and metronomic chemotherapy using PTX@Ce6 NPs (+) induced a strong immune memory response that effectively suppressed the tumor recurrence in mice.

We investigated the natural metastasis of 4T1 tumor cells after various treatments, according to the treatment schedule shown in Figure 3a. On day 24, the lungs from all test mice were excised to assess the differences in tumor metastasis between the PBS and treatment groups. As shown in Figure 7f, the lungs from the PBS group had eight tumor nodules (marked with black circles), the lungs from the PTX NP group had two tumor nodules, and the lungs from the Ce6 NPs (+) group had only one tumor nodule, indicating that both treatment modes had a preventative effect on lung metastasis. Notably, combination therapy based on PTX@Ce6 NPs completely prevented the lung metastasis of 4T1 tumors, and no nodules were found in the lungs of this group. Representative lungs were sectioned and stained with H&E to visualize the metastatic area, as shown in Figure 7g. These results are consistent with those obtained in the tumor nodules.

Figure 7. (a) Schedule for rechallenged tumors by combination therapy based on PTX@Ce6 NPs (+). (b) Volume growth curves of rechallenged tumors. (c) Survival rates of mice in each of the two groups ($n = 10$). (d) Representative frequency of T_{EM} cells in the spleens of mice. (e) Quantitative frequency of T_{EM} cells. (f) Representative images of tumor nodules in the lungs. (g) Images of lung sections stained with H&E. (h) Masses of rechallenged tumors.

4. CONCLUSIONS

In summary, we demonstrated the preparation of core−shell PTX@Ce6 NPs with a 100% drug loading rate using a two-step reprecipitation method in this study. In the core−shell PTX@Ce6 nanostructure, the toxic PTX core was embedded into a nontoxic Ce6 shell. PTX in ultra-low doses mainly acts as an immunomodulator to differentiate MDSCs into mature DCs, whereas Ce6 releases $^1O_2$ to kill the tumor cells. PDT and metronomic chemotherapy induced ICD in tumor cells. Mature DCs and tumor-associated antigens released by ICD induced the proliferation of CD8$^+$ cells in the tumor microenvironment, which further killed the residual cancer cells after PDT. In this study, tumors were eradicated with 100% tumor inhibition rate via combination therapy with PDT and metronomic chemotherapy using PTX@Ce6 NPs. Tumor recurrence and metastasis were also effectively inhibited by the

combination therapy. Moreover, the combination therapy showed high biosafety in the treatment of mice with 4T1 tumors.

■ AUTHOR INFORMATION

Corresponding Authors

Rui Zhang — *School of Public Health, Jilin University, Changchun 130021 Jilin, China;* ⊙ orcid.org/0000-0003-2398-8309; Email: zhangrui625827@jlu.edu.cn

Juan Li — *School of Public Health, Jilin University, Changchun 130021 Jilin, China;* Email: li_juan@jlu.edu.cn

Authors

Mengxuan Li — *School of Public Health, Jilin University, Changchun 130021 Jilin, China*

Ge Cheng — *School of Public Health, Jilin University, Changchun 130021 Jilin, China*

Complete contact information is available at:
https://pubs.acs.org/10.1021/acsomega.2c06578

Author Contributions

[†]M.L. and G.C. contributed equally to this work.

Notes

The authors declare no competing financial interest.

■ ACKNOWLEDGMENTS

■ REFERENCES

(1) Liu, Y.; Xu, Y.; Zhang, Z.; Huo, Y.; Chen, D.; Ma, W.; Sun, K.; Tonga, G. Y.; Zhou, G.; Kohane, D. S.; Tao, K. A Simple, Yet Multifunctional, Nanoformulation for Eradicating Tumors and Preventing Recurrence with Safely Low Administration Dose. *Nano Lett.* **2019**, *19*, 5515−5523.

(2) Song, J.; Yang, X.; Jacobson, O.; Huang, P.; Sun, X.; Lin, L.; Yan, X.; Niu, G.; Ma, Q.; Chen, X. Multimodal-Imaging-Guided Cancer Phototherapy by Versatile Biomimetic Theranostics with UV and γ-Irradiation Protection. *Adv. Mater.* **2016**, *28*, 3273−3279.

(3) Wang, S.; Huang, P.; Chen, X. Hierarchical Targeting Strategy for Enhanced Tumor Tissue Accumulation/Retention and Cellular Internalization. *Adv. Mater.* **2016**, *28*, 7340−7364.

(4) Mura, S.; Nicolas, J.; Couvreur, P. Stimuli-responsive nano-carriers for drug delivery. *Nat. Mater.* **2013**, *12*, 991−1003.

(5) Kamaly, N.; Yameen, B.; Wu, J.; Farokhzad, O. C. Degradable Controlled-Release Polymers and Polymeric Nanoparticles: Mechanisms of Controlling Drug Release. *Chem. Rev.* **2016**, *116*, 2602−2663.

(6) Li, F.; Du, Y.; Liu, J.; Sun, H.; Wang, J.; Li, R.; Kim, D.; Hyeon, T.; Ling, D. Responsive Assembly of Upconversion Nanoparticles for pH-Activated and Near-Infrared-Triggered Photodynamic Therapy of Deep Tumors. *Adv. Mater.* **2018**, *30*, No. e1802808.

(7) Ouyang, J.; Xie, A.; Zhou, J.; Liu, R. C.; Wang, L. Q.; Liu, H. J.; Kong, N.; Tao, W. Minimally Invasive Nanomedicine: Nanotechnology in Photo-/Ultrasound-/Radiation−/Magnetism-mediated Therapy and Imaging. *Chem. Soc. Rev.* **2022**, *51*, 4996−5041.

(8) Sun, Q.; Zhou, Z.; Qiu, N.; Shen, Y. Rational Design of Cancer Nanomedicine: Nanoproperty Integration and Synchronization. *Adv. Mater.* **2017**, *29*, No. 1606628.

(9) Bjornmalm, M.; Thurecht, K. J.; Michael, M.; Scott, A. M.; Caruso, F. Bridging Bio−Nano Science and Cancer Nanomedicine. *ACS Nano* **2017**, *11*, 9594−9613.

(10) Rosenblum, D.; Joshi, N.; Tao, W.; Karp, J. M.; Peer, D. Progress and challenges towards targeted delivery of cancer therapeutics. *Nat. Commun.* **2018**, *9*, 1410.

(11) Min, Y.; Caster, J. M.; Eblan, M. J.; Wang, A. Z. Clinical Translation of Nanomedicine. *Chem. Rev.* **2015**, *115*, 11147−11190.

(12) Cheng, Z.; Al Zaki, A.; Hui, J. Z.; Muzykantov, V. R.; Tsourkas, A. Multifunctional Nanoparticles: Cost Versus Benefit of Adding Targeting and Imaging Capabilities. *Science* **2012**, *338*, 903−910.

(13) Feng, B.; Niu, Z.; Hou, B.; Zhou, L.; Li, Y.; Yu, H. Enhancing Triple Negative Breast Cancer Immunotherapy by ICG-Templated Self-Assembly of Paclitaxel Nanoparticles. *Adv. Funct. Mater.* **2020**, *30*, No. 1906605.

(14) Xu, C. F.; Iqbal, S.; Shen, S.; Luo, Y. L.; Yang, X.; Wang, J. Development of "CLAN" Nanomedicine for Nucleic Acid Therapeutics. *Small* **2019**, *15*, No. 1900055.

(15) Chung, J. E.; Tan, S.; Gao, S. J.; Yongvongsoontorn, N.; Kim, S. H.; Lee, J. H.; Choi, H. S.; Yano, H.; Zhuo, L.; Kurisawa, M.; Ying, J. Y. Self-Assembled Micellar Nanocomplexes Comprising Green Tea Catechin Derivatives and Protein Drugs for Cancer Therapy. *Nat. Nanotechnol.* **2014**, *9*, 907.

(16) Xing, R.; Zou, Q.; Yuan, C.; Zhao, L.; Chang, R.; Yan, X. Self-Assembling Endogenous Biliverdin as a Versatile Near-Infrared Photothermal Nanoagent for Cancer Theranostics. *Adv. Mater.* **2019**, *31*, No. 1900822.

(17) Park, J.; Sun, B.; Yeo, Y. Albumin-coated nanocrystals for carrier-free delivery of paclitaxel. *J. Controlled Release* **2017**, *263*, 90.

(18) Castano, A. P.; Demidova, T. N.; Hamblin, M. R. Mechanisms in Photodynamic Therapy: Part One——Photosensitizers, Photochemistry and Cellular Localization. *Photodiagn. Photodyn. Ther.* **2004**, *1*, 279−293.

(19) Xie, Z.; Cai, X.; Sun, C.; Liang, S.; Shao, S.; Huang, S.; Cheng, Z.; Pang, M.; Xing, B.; Al Kheraif, A. A.; Lin, J. O_2-Loaded pH-Responsive Multifunctional Nanodrug Carrier for Overcoming Hypoxia and Highly Efficient Chemo-Photodynamic Cancer Therapy. *Chem. Mater.* **2019**, *31*, 483−490.

(20) Miura, K.; Wen, Y.; Tsushima, M.; Nakamura, H. Photodynamic Therapy by Glucose Transporter 1-Selective Light Inactivation. *ACS Omega* **2022**, *7*, 34685−34692.

(21) Pham, T. C.; Nguyen, V. N.; Choi, Y.; Lee, S.; Yoon, J. Recent Strategies to Develop Innovative Photosensitizers for Enhanced Photodynamic Therapy. *Chem. Rev.* **2021**, *121*, 13454−13619.

(22) Gallaga-González, U.; Morales-Avila, E.; Torres-García, E.; Estrada, J. A.; Díaz-Sánchez, L. E.; Izquierdo, G.; Aranda-Lara, L.; Isaac-Olivé, K. Photoactivation of Chemotherapeutic Agents with Cerenkov Radiation for Chemo-Photodynamic Therapy. *ACS Omega* **2022**, *7*, 23591−23604.

(23) Yao, Q. C.; Fan, J. L.; Long, S. R.; Zhao, X. Z.; Li, H. D.; Du, J. J.; Shao, K.; Peng, X. J. The concept and examples of type-III photosensitizers for cancer photodynamic therapy. *Chem* **2022**, *8*, 197−209.

(24) Li, X.; Wang, Y.; Shi, Q.; Zhen, N.; Xue, J.; Liu, J.; Dongfang Zhou, D.; Zhang, H. Zein-Based Nanomedicines for Synergistic Chemodynamic/Photodynamic Therapy. *ACS Omega* **2022**, *7*, 29256−29265.

(25) Spring, B. Q.; Kessel, D. 3D Culture Models of Malignant Mesothelioma Reveal a Powerful Interplay Between Photodynamic Therapy and Kinase Suppression Offering Hope to Reduce Tumor Recurrence. *Photochem. Photobiol.* **2019**, *95*, 462−463.

(26) Kampan, N. C.; Madondo, M. T.; McNally, O. M.; Quinn, M.; Plebanski, M. Paclitaxel and Its Evolving Role in the Management of Ovarian Cancer. *BioMed Res. Int.* **2015**, *2015*, No. 413076.

(27) Kumar, A.; Hoskins, P. J.; Tinker, A. V. Dose-dense Paclitaxel in Advanced Ovarian Cancer. *Clin. Oncol.* **2015**, *27*, 40−47.

(28) Thapa, P.; Li, M.; Bio, M.; Rajaputra, P.; Nkepang, G.; Sun, Y.; Woo, S.; You, Y. Far-red Light-activatable Prodrug of Paclitaxel for the Combined Effects of Photodynamic Therapy and Site-specific Paclitaxel Chemotherapy. *J. Med. Chem.* **2016**, *59*, 3204−3214.

(29) Chen, Y.; Chang, M.; Cheng, W. Metronomic Chemotherapy and Immunotherapy in Cancer Treatment. *Cancer Lett.* **2017**, *400*, 282−292.

(30) Michels, T.; Shurin, G. V.; Naiditch, H.; Sevko, A.; Umansky, V.; Shurin, M. R. Paclitaxel Promotes Differentiation of Myeloidderived Suppressor Cells into Dendritic Cells *in vitro* in a TLR4-Independent Manner. *J. Immunotoxicol.* **2012**, *9*, 292−300.

(31) Condamine, T.; Gabrilovich, D. I. Molecular Mechanisms Regulating Myeloid-Derived Suppressor Cell Differentiation and Function. *Trends Immunol.* **2010**, *32*, 19−25.

(32) Chen, R.; Zhang, J.; Wang, Y.; Chen, X.; Zapien, J. A.; Lee, C. S. Graphitic Carbon Nitride Nanosheet@Metal−Organic Framework Core−Shell Nanoparticles for Photo-Chemo Combination Therapy. *Nanoscale* **2015**, *7*, 17299.

(33) Chen, W.; Ouyang, J.; Liu, H.; Chen, M.; Zeng, K.; Sheng, J.; Liu, Z.; Han, Y.; Wang, L.; Li, J.; Deng, L.; Liu, Y. N.; Guo, S. Black Phosphorus Nanosheet-Based Drug Delivery System for Synergistic Photodynamic/Photothermal/Chemotherapy of Cancer. *Adv. Mater.* **2017**, *29*, No. 1603864.

(34) Yang, X.; Shi, X.; Zhang, Y.; Xu, J.; Ji, J.; Ye, L.; Yi, F.; Zhai, G. Photo-Triggered Self-Destructive ROS-Responsive Nanoparticles of High Paclitaxel/Chlorin e6 Co-Loading Capacity for Ynergetic chemo-photodynamic therapy. *J. Controlled Release* **2020**, *323*, 333−349.

(35) Martella, E.; Ferroni, C.; Guerrini, A.; Ballestri, M.; Columbaro, M.; Santi, S.; Sotgiu, G.; Serra, M.; Davide Mari Donati, D. M.; Lucarelli, E.; Varchi, G.; Duchi, S. Functionalized Keratin as Nanotechnology-Based Drug Delivery System for the Pharmacological Treatment of Osteosarcoma. *Int. J. Mol. Sci.* **2018**, *19*, 3670.

(36) Martella, E.; Dozza, B.; Ferroni, C.; Obeyok, C. O.; Guerrini, A.; Tedesco, D.; Manet, L.; Sotgiu, G.; Columbaro, M.; Ballestri, M.; Martini, L.; Fini, M.; Lucarelli, E.; Varchi, G.; Duchi, S. Two Beats One: Osteosarcoma Therapy with Light-Activated and Chemo-Releasing Keratin Nanoformulation in a Preclinical Mouse Model. *Pharmaceutics* **2022**, *14*, 677.

(37) He, Z.; Jiang, H.; Zhang, X.; Zhang, H.; Cui, Z.; Sun, L.; Li, H.; Qian, J.; Ma, J.; Huang, J. Nano-Delivery Vehicle Based on Chlorin E6, Photodynamic Therapy, Doxorubicin Chemotherapy Provides Targeted Treatment of HER-2 Negative, $\alpha\nu\beta$3-Positive Breast Cancer. *Pharmacol. Res.* **2020**, *160*, No. 105184.

(38) Liang, R.; Liu, L.; He, H.; Chen, Z.; Han, Z.; Luo, Z.; Wu, Z.; Zheng, M.; Ma, Y.; Cai, L. Oxygen-Boosted Immunogenic Photodynamic Therapy with Gold Nanocages@Manganese Dioxide to Inhibit Tumor Growth and Metastases. *Biomaterials* **2018**, *177*, 149−160.

(39) Liu, X.; Su, H.; Shi, W.; Liu, Y.; Sun, Y.; Ge, D. Functionalized Poly(pyrrole-3-carboxylic acid) Nanoneedles for Dual Imaging Guided PDT/PTT Combination Therapy. *Biomaterials* **2018**, *167*, 177−190.

(40) Wang, Y.; Zhao, J.; Chen, Z.; Zhang, F.; Wang, Q.; Guo, W.; Wang, K.; Lin, H.; Qu, F. Construct of MoSe$_2$/Bi$_2$Se$_3$ Nanoheterostructure: Multimodal CT/PT Imaging-Guided PTT/PDT/Chemotherapy for Cancer Treating. *Biomaterials* **2019**, *217*, No. 119282.

(41) Yu, W.; Wang, Y.; Zhu, J.; Jin, L.; Liu, B.; Xia, K.; Wang, J.; Gao, J.; Liang, C.; Tao, H. Autophagy Inhibitor Enhance ZnPc/BSA Nanoparticle Induced Photodynamic Therapy by Suppressing PD-L1 Expression in Osteosarcoma Immunotherapy. *Biomaterials* **2019**, *192*, 128−139.

(42) Gabrilovich, D. I.; Nagaraj, S. Myeloid-Derived Suppressor Cells as Regulators of the Immune System. *Nat. Rev. Immunol.* **2009**, *9*, 162−174.

(43) Végran, A. L. F.; Ladoire, S.; Ghiringhelli, F. Restoration of Antitumor Immunity Through Selective Inhibition of Myeloid Derived Suppressor Cells by Anticancer Therapies. *Curr. Mol. Med.* **2011**, *11*, 365−372.